TM-TE DECOMPOSITION OF POWER LOSSES IN MULTI-STRANDED LITZ-WIRES USED IN ELECTRONIC DEVICES

C. Carretero[1,*], J. Acero[1], and R. Alonso[2]

[1]Dep. Ingeniería Electrónica y Comunicaciones, Universidad de Zaragoza, María de Luna, 1, 50018 Zaragoza, Spain

[2]Dep. Física Aplicada, Universidad de Zaragoza, Pedro Cerbuna, 12, 50009 Zaragoza, Spain

Abstract—Efficiency often constitutes the main goal in the design of a power system because the minimization of power losses in the magnetic components implies better and safer working conditions. The primary source of losses in a magnetic power component is usually associated with the current driven by the wire, which ranges from low to medium frequencies. New power system tendencies involve increasing working frequencies in order to reduce the size of devices, thus reducing costs. However, optimal design procedures involve increasingly complex solutions for improving system performance. For instance, using litz-type multi-stranded wires which have an internal structure to uniformly share the current between electrically equivalent strands, reducing the total power losses in the windings. The power losses in multi-stranded wires are generally classified into conduction losses and proximity losses due to currents induced by a magnetic field external to the strand. Both sources of loss have usually been analyzed independently, assuming certain conditions in order to simplify the derivation of expressions for calculating the correct values. In this paper, a unified analysis is performed given that both power losses are originated by the electromagnetic fields arising from external sources where the wire is immersed applying the decomposition into transversal magnetic (TM) and transversal electric (TE) components. The classical power losses, the so called conduction and proximity losses, can be calculated considering the TM modes under certain conditions. In addition, a new proximity loss contribution emerges from the TE modes under similar conditions.

1. INTRODUCTION

Many models have been developed over the years to calculate power losses produced in windings in order to optimize magnetic power components, such as transformers and inductors. Early results were obtained from analytical models assuming certain conditions in order to simplify the problem. Power loss expressions considering straight cylindrical wires are provided in [1] for different excitations associated with different kinds of power losses. For instance, conduction power losses are associated with an axial electric field whereas proximity losses are related with an external transversal magnetic field. This book provides analytical solutions for simplified systems based on Bessel functions arising from their rotational symmetry. Reviews of several techniques employed in the estimation of power losses in the wires of transformers and inductors are provided in [2–4] with concise evaluations being made by comparison. The method described in [5] is widely used in the design of foil transformers because the power losses are derived from a simplified 1-D modeling of the electromagnetic field, considerably reducing the geometrical complexity and consequently simplifying the numerical calculation. This paper constitutes the basis of a large number of subsequent works [6, 7], but assuming restrictive approximations.

In more recent years, preferred solutions have involved the calculation of the electromagnetic fields of systems by means of analytical or numerical calculations with the power losses being subsequently derived in a straightforward manner from the analytical expressions. The basic structure of typical wires used in high frequency power applications are packed bundles of many small circular cross-section strands made of a good conductor, for instance, copper or aluminum. Multi-stranded wires can be classified depending on the braid of the construction as twisted multi-stranded wires, with the strands occupying a constant distance to the wire axis [8], and litz-type wire, with strands exhibiting radial and azimuthal transposition [9].

The losses in each strand can be analytically calculated by means of two-dimensional equations obtained for a simplified geometry of a straight homogeneous cylinder immersed in a uniform field. This approach has been followed by many authors arriving at expressions based on Bessel functions which are applied to calculate the losses in litz-wires, as may be seen in [10–16]. It should be noted that the solution can be achieved either by considering physical external field excitations [17, 18], or from a Helmholtz potential point of view [19, 20]. Alternatively, simpler expressions can be obtained neglecting the influence of the strand induced currents over the external fields, in

other words, the electromagnetic field is not distorted by the presence of the strand. Equivalently, in the latter case, a low-frequency approach is assumed with respect to the previous methodology, as followed in [21–23].

The expressions given in the preceding papers include the electromagnetic fields obtained either by means of analytical techniques [24, 25], or by using numerical methods, in particular methods based on finite elements [23–31].

Litz-wires generally consist of a large number of small size strands, thus the effect of an individual strand in the electromagnetic behavior of the system can be neglected because the fields are slightly distorted. However, their effects are included by addition of the power loss contribution in the equivalent resistance of the device. Moreover, the electromagnetic field where the strand is immersed can be considered external to the strand due to the sources being outside its cylindrical volume. As a consequence, the well-know decomposition into TM and TE components with respect to an arbitrary axis can be applied, as is given in [32–37], to split the external field along the longitudinal axis of the strand. Each component of the decomposition individually contributes to the total power losses induced in the cylindrical conductor, as appears for the TM modes in [38] and for the TE modes in [39]. In this paper, the classical contributions to power losses, namely proximity and conduction losses, are associated with the zeroth and first order TM modes, whereas the zeroth order TE mode concerns the proximity effect due to an external longitudinal magnetic field.

2. LOSS MODELING IN CYLINDRICAL STRANDS

The internal structure of a multi-stranded wire consists of n_0 cylindrical strands of circular cross-section made of a material with high electrical conductivity, usually copper or aluminum. Magnetic materials are not suitable for building wires due to the increase in power losses. Generally, the strands are braided in a litz-wire structure in order to minimize the total power losses. This is because such structure, shown in Figure 1, produces greater equivalence between strands and therefore the strands tend to carry the same current.

The analysis of power losses is performed assuming the following conditions. In the first place, a single strand model is developed in order to simplify the treatment. The strand to be analyzed is a straight cylinder of infinite length immersed in the external field. The effect of the strand curvature is therefore neglected. The analysis can be extended to multi-stranded systems by applying the equivalence
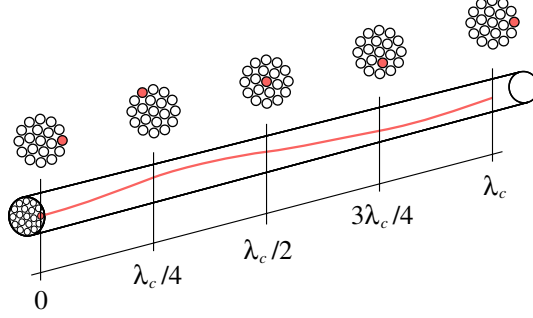
Figure 1. Structure of the litz-wire showing the trajectory of a strand with a characteristic length λ_c.

between strands. Second, the power losses arise from the external electromagnetic field which model the effect of the remainder of the system where the strand is placed. The strand is therefore assumed to be inside a volume with no field sources, thus the effects of the fields are decoupled from their sources. The decomposition into TM and TE components of the fields is assumed to obtain the complete description of the external field. The longitudinal direction of the strand $\hat{\mathbf{z}}$ is chosen to perform this decomposition. Moreover, the magneto-quasistatic approach is assumed to simplify the analysis because the radiation contribution is slight with respect to the diffusion effects of the field inside the conductor [40], or, equivalently, the displacement current $\mathbf{J}_d$ in the system is negligible compared to the induced currents $\mathbf{J}_c$ in the strand at the working frequencies of the power devices ranging from dc to several MHz. Finally, the power losses are associated with induced current in the strands because the hysteresis effects can be neglected in the media with permeability values close to vacuum permeability μ_0, as occurs for copper or aluminum.

The TM-TE decomposition of the electromagnetic field in the free space where the strand is immersed is performed by means of the longitudinal components $E_z^0(\mathbf{r})$ and $H_z^0(\mathbf{r})$, respectively, which can be expanded in a Taylor series with respect to the reference position $\mathbf{r}_i$, as is shown as follows:

$$E_z^0(\mathbf{r}) = \sum_{n=0}^{\infty} \frac{1}{n!} \left(\mathbf{r}' \cdot \nabla\right)^n E_z^0(\mathbf{r}_i) \quad \text{(TM modes)}, \tag{1}$$

$$H_z^0(\mathbf{r}) = \sum_{i=0}^{\infty} \frac{1}{n!} \left(\mathbf{r}' \cdot \nabla\right)^n H_z^0(\mathbf{r}_i) \quad \text{(TE modes)}, \tag{2}$$

where $\mathbf{r}'$ is defined as $\mathbf{r} - \mathbf{r}_i$.

The terms of the expansion applied to the longitudinal electric field $E_z^0(\mathbf{r})$, in (1) are:

$$E_z^0(\mathbf{r}) = E_z^0(\mathbf{r}_i) + \left(\mathbf{r}' \cdot \nabla\right) E_z^0(\mathbf{r}_i) + \ldots, \tag{3}$$

where the operator ∇ may be divided into transversal ∇_t and longitudinal $\hat{\mathbf{z}}\partial_z$ components [42], where the transversal component ∇_t can be expressed in the appropriate coordinate framework, for instance, a rectangular or polar coordinate system. Furthermore, the spatial vector $\mathbf{r}'$ is decomposed into the transversal $\mathbf{t}'$ and the longitudinal $\mathbf{z}'$ vectors. Consequently, we obtain that (3) can be rewritten as:

$$E_z^0(\mathbf{r}) = E_z^0(\mathbf{r}_i) + \left(\mathbf{t}' \cdot \nabla_t\right) E_z^0(\mathbf{r}_i) + z' \cdot \partial_z E_z^0(\mathbf{r}_i) + \ldots \tag{4}$$

The first term in (4) is a uniform longitudinal electric field $E_z^0(\mathbf{r}_i)\hat{\mathbf{z}}$ constituting the main source of the conduction losses in the strands because the conduction current density $\mathbf{J}_c$ equal to $\sigma E_z^0(\mathbf{r}_i)\hat{\mathbf{z}}$ dissipates energy. The surface integral of $\mathbf{J}_c$ in the cross-section area is the current I_0 carried by the strand.

The second term in (4) is an anti-symmetric electric field with respect to the plane at the position $\mathbf{r}_i$ with normal directed along the transversal gradient of the electric field. This contribution is associated with a uniform transversal magnetic field $\mathbf{H}_t^0(\mathbf{r})$, which is therefore the source of the classical proximity losses. The relationship between the term $(\mathbf{t}' \cdot \nabla_t)E_z^0(\mathbf{r}_i)\hat{\mathbf{z}}$ and $\mathbf{H}_t^0(\mathbf{r})$ can be carried out applying Maxwell's equation:

$$\nabla \times \mathbf{E}(\mathbf{r}, t) = -\partial_t \mathbf{B}(\mathbf{r}, t). \tag{5}$$

In the preceding expression, the electric field $\mathbf{E}(\mathbf{r})$ and the magnetic induction field $\mathbf{B}(\mathbf{r})$ are equal to $(\mathbf{t}'\cdot\nabla_t)E_z^0(\mathbf{r}_i)\hat{\mathbf{z}}$ and $\mu_0\mathbf{H}_t^0(\mathbf{r})$, respectively. Moreover, the operator ∂_t is replaced by the operator $j\omega$ because the harmonic approach will be implicitly applied, assuming $e^{j\omega t}$ time dependence. As a result, we obtain the following relationship:

$$\nabla \times \left(\hat{\mathbf{z}}\left(\mathbf{t}' \cdot \nabla_t\right) E_z(\mathbf{r}_i)\right) = -j\omega\mu_0\mathbf{H}_t^0(\mathbf{r}). \tag{6}$$

Rearranging the preceding expression, we have:

$$-\hat{\mathbf{z}} \times \nabla_t \left(\left(\mathbf{t}' \cdot \nabla_t\right) E_z(\mathbf{r}_i)\right) = -j\omega\mu_0\mathbf{H}_t^0(\mathbf{r}). \tag{7}$$

Performing the vector product by the unitary vector $\hat{\mathbf{z}}$ and afterwards applying the scalar product by the vector $\hat{\mathbf{t}}$ in both sides of the equation, the following equivalence is obtained:

$$\left(\mathbf{t}' \cdot \nabla_t\right) E_z(\mathbf{r}_i) = -j\omega\mu_0 \left(\hat{\mathbf{z}} \times \mathbf{H}_t^0(\mathbf{r})\right) \cdot \mathbf{t}'. \tag{8}$$

Consequently, the second term in (4) can be evaluated in a straightforward manner including the uniform transversal magnetic field $\mathbf{H}_t^0(\mathbf{r})$ in (8).

The last term shown in (4) concerns the longitudinal first order variation of the longitudinal electric field related with the electric charge density in the strand, modifying the current density along the wire, but without associated current densities constituting new power loss sources. A further analysis can be performed considering higher order terms, but the results would be beyond the scope of this paper. In conclusion, the zeroth and first order TM modes originated the classical behavior for the conduction resistance and proximity losses due to the uniform longitudinal electric field $E_z^0(\mathbf{r}_i)\hat{\mathbf{z}}$ and transversal magnetic field $\mathbf{H}_t^0(\mathbf{r})$, respectively.

The complete decomposition of the external electromagnetic field is given by the TM-TE decomposition. The power losses in the strands are typically accounted for considering TM modes only, but TE modes are included in order to achieve a complete description of the power losses. The zeroth term in (2) is a uniform longitudinal magnetic field $H_z^0(\mathbf{r}_i)\hat{\mathbf{z}}$. Higher order terms can be neglected because their contribution to the losses is slight. Note that the zeroth order TE mode constitutes a new proximity loss source.

3. ANALYTICAL EXPRESSIONS OF POWER LOSSES

The power loss expressions can be obtained starting with the governing equation applied to the corresponding transversal representation of the external field. The cylindrical coordinate system formulation is employed to work out the solution due to the geometrical symmetry of the single strand system.

TM mode fields obey the following scalar equation [38]:

$$\nabla^2 E_z(\mathbf{r}) - j\omega\mu\sigma E_z(\mathbf{r}) = 0, \tag{9}$$

being μ and σ, the magnetic permeability and electric conductivity of the different media, respectively. Moreover, the magneto-quasistatic approach [40] has been applied because the radiation can be neglected with respect to the induced current effects, obtaining an electromagnetic diffusion equation [41]. The solution should be worked out applying the boundary condition for the electric and magnetic field at the surface of the strand and, additionally, the far away fields must converge to the considered external field term. The general solution is based on Bessel and trigonometric functions [42].

Considering the zeroth order term of (4), by solving (9), we obtain [1]:

$$E_z(\mathbf{r}) = \frac{J_0\left((j-1)\rho/\delta\right)}{J_0\left((j-1)r_0/\delta\right)} E_z^0(\mathbf{r}_i) \quad \rho \le r_0, \tag{10}$$

and

$$E_z(\mathbf{r}) = E_z^0(\mathbf{r}_i) \quad \rho > r_0, \tag{11}$$

where δ is the strand penetration depth defined as $\sqrt{2/(\omega\mu\sigma)}$, and ρ is the radial distance with respect to the position $\mathbf{r}_i$ located at the center of the strand. Note that the external uniform field is constant in the medium surrounding the strand, but its amplitude diminishes when it penetrates inside the conductive media.

The first order TM term associated with the second term in (4) obeys the following solution [19]:

$$E_z(\mathbf{r}) = 2\frac{1-j}{\sigma\delta}\frac{J_1\left((j-1)\rho/\delta\right)}{J_0\left((j-1)\rho/\delta\right)}\sin(\varphi-\varphi_0)H_t^0 \quad \rho \le r_0, \tag{12}$$

and

$$E_z(\mathbf{r}) = \left[2\frac{1-j}{\sigma\delta}\frac{J_1((j-1)\rho/\delta)}{J_0((j-1)\rho/\delta)}\frac{r_0}{\rho} + j\omega\mu_0\left(\rho - \frac{r_0^2}{\rho}\right)\right]\sin(\varphi-\varphi_0)H_t^0$$
$$\rho > r_0, \tag{13}$$

where H_t^0 is the magnitude of the transversal magnetic field $\mathbf{H}_t^0(\mathbf{r}_i)$ and φ_0 is the azimuthal coordinate φ of the vector $\hat{\mathbf{z}} \times \mathbf{H}_t^0(\mathbf{r}_i)$ expressed in the cylindrical reference system. The magnetic field is influenced by the induced currents in the vicinity of the strand.

Both power loss contributions can be associated with resistive loss terms arising from the current densities due to the internal electric field $\mathbf{E}_z(\mathbf{r})$ in (10) and (12) for the conduction and proximity losses, respectively. These resistive contributions are analyzed as follows. It should be noted that the reference coordinate $\mathbf{r}_i$ has been chosen in such a way as to avoid the contribution of the second term in (4) to the total current carried by the strand. Thus, the conduction resistance can be calculated from the ratio between the voltage per unit of length equal to $E_z^0(\mathbf{r}_i)$ and the current I_0 carried by the strand. Integrating the current density $\sigma E_z^0(\mathbf{r}_i)\hat{\mathbf{z}}$ flowing through the cross-section area, we obtain the current I_0 driven by the cylinder [19]:

$$I_0 = \frac{2\pi r_0\delta\sigma J_1\left((j-1)r_0/\delta\right)}{(j-1)J_0\left((j-1)r_0/\delta\right)}E_z^0(\mathbf{r}_i). \tag{14}$$

The conduction resistance per unit length $R_{cond,\,u.l.}$ is defined as the real part of the ratio between the voltage per unit length, given by the amplitude of $E_z^0(\mathbf{r}_i)$, and the current I_0, hence:

$$R_{cond,\,u.l.} = \frac{1}{\pi r_0^2\sigma}\Phi_{cond}(r_0/\delta), \tag{15}$$

where the factor $\Phi_{cond}(r_0/\delta)$ is defined as:

$$\Phi_{cond}(r_0/\delta) = \Re e\left((j-1)\frac{r_0}{\delta}\frac{J_0\left((j-1)r_0/\delta\right)}{J_1\left((j-1)r_0/\delta\right)}\right), \tag{16}$$
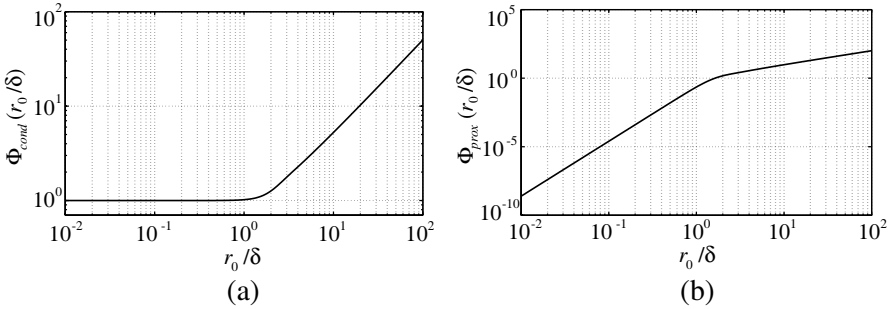
Figure 2. Representation of conduction and proximity factor depending on the ratio r_0/δ between the radius of the strand and the penetration depth. (a) $\Phi_{cond}(r_0/\delta)$. (b) $\Phi_{prox}^{low}(r_0/\delta)$.

Note that (15), which is depicted in Figure 2(a), includes the skin effect accounted by the factor $\Phi_{cond}(r_0/\delta)$ depending on the ratio r_0/δ.

The second term in (4) originates the classical proximity power losses in the strand which may be evaluated by integrating the density factor $\frac{1}{2}\mathbf{E} \cdot \mathbf{J}^*$, where $\mathbf{E}$ is provided in (12), obtaining the losses per unit length of the strand due to a transversal magnetic field [19]:

$$P_{prox\,t,\,u.l.} = \frac{2\pi}{\delta}\Phi_{prox}(r_0/\delta)\left|H_t^0\right|^2, \tag{17}$$

where $|H_t^0|$ is the amplitude of the external magnetic field $\mathbf{H}_t^0(\mathbf{r}_i)$. The factor $\Phi_{prox}(r_0/\delta)$, shown in Figure 2(b), is provided by many authors in a form depending on Kelvin functions, as it appears in [1, 43], but the mathematical equivalent expression given in [27, 29] is preferred because it is more compact, as can be seen as follows:

$$\Phi_{prox}(r_0/\delta) = \Re e\left(j\left(\frac{r_0}{\delta}\right)^2 \frac{J_2\left((j-1)r_0/\delta\right)}{J_0\left((j-1)r_0/\delta\right)}\right), \tag{18}$$

In many cases, the external magnetic field arises from a certain well defined current amplitude I, for instance, in magnetic devices for power applications immersed in the self-magnetic field. Consequently, we are able to define the proximity resistance per unit length by means of the relationship $P_{prox\,t,\,u.l.} = \frac{1}{2}R_{prox\,t,\,u.l.}I^2$:

$$R_{prox\,t,\,u.l.} = \frac{4\pi}{\delta}\Phi_{prox}(r_0/\delta)\bar{H}_t^2, \tag{19}$$

where $\bar{H}_t$ is the normalized amplitude of the external transversal magnetic field $|H_t^0|$ divided by the total current I carried by the n_0 strands of the system.

The zeroth order TE mode in (2) is associated with a uniform longitudinal magnetic field H_z^0. TE modes are governed by the corresponding scalar equation with the structure of (9) substituting E_z by H_z. In this case, the first TE term solution has the following form [39]:

$$H_z(\mathbf{r}) = \frac{1}{\sigma} \frac{J_0\left((j-1)\rho/\delta\right)}{J_0\left((j-1)r_0/\delta\right)} H_z^0(\mathbf{r}_i) \quad \rho \le r_0, \tag{20}$$

and

$$H_z(\mathbf{r}) = H_z^0(\mathbf{r}_i) \quad \rho > r_0. \tag{21}$$

The longitudinal magnetic field of the preceding equation can be associated with a transversal electric field inside the conductor by means of the identity $\mathbf{E}(\mathbf{r}) = \frac{1}{\sigma}\hat{\mathbf{z}} \times \nabla H_z(\mathbf{r})$ derived from the Maxwell's equations under the magneto-quasistatic approach $\nabla \times \mathbf{H}(\mathbf{r}) = \mathbf{J}(\mathbf{r})$, where the current density is $\sigma\mathbf{E}(\mathbf{r})$. Thus, we have:

$$\mathbf{E}(\mathbf{r}) = \frac{j-1}{\sigma\delta} \frac{J_1\left((j-1)\rho/\delta\right)}{J_0\left((j-1)r_0/\delta\right)} H_z^0(\mathbf{r}_i)\hat{\varphi} \quad \rho \le r_0, \tag{22}$$

The additional TE mode contribution $P_{prox\,z,\,u.l.}$ to the proximity power losses due to a uniform longitudinal external magnetic field $H_z^0(\mathbf{r}_i)$ can also be obtained integrating the factor $\mathbf{E}\cdot\frac{1}{2}\mathbf{J}^*$ in the volume of the unit length of the strand. Afterwards, the proximity resistance due to a longitudinal magnetic field $R_{prox\,z,\,u.l.}$ is obtained:

$$R_{prox\,z,\,u.l.} = \frac{2\pi}{\sigma} \Phi_{prox}(r_0/\delta)\bar{H}_z^2, \tag{23}$$

where $\bar{H}_z$ is the normalized amplitude of the external longitudinal magnetic field $|H_z^0(\mathbf{r}_i)|$ divided by the total current I carried by the system.

According to (19) and (23), proximity power losses due to transversal or longitudinal magnetic fields are characterized by the following aspects. The frequency dependence of the proximity resistance is accounted for by the ratio r_0/δ. The dependence functions are the same $\Phi_{prox}(r_0/\delta)$ for either transversal or longitudinal magnetic fields. The proximity power losses for a transversal magnetic field doubles the proximity power losses for a longitudinal magnetic field of equal amplitude and frequency acting in a given strand, thus, $2R_{prox\,z,\,u.l.} = R_{prox\,t,\,u.l.}$ because the induced current densities in both cases are related by a $2\sin(\varphi - \varphi_0)$ factor. Moreover, owing to the orthogonality between the sources, the total proximity resistance can be calculated by the addition of the two contributions.

4. LOW- AND HIGH-FREQUENCY ANALYSIS

In many cases, it is worth obtaining simplified expressions that approach the exact function to evaluate the power losses based on extreme behavior of the system. The losses in the strand can be approached taking into account the dependence with respect to the frequency of the excitation, being possible to distinguish between the low frequency and the high frequency limit as is pointed out in [46] for different strand geometries.

In the low frequency limit, the power losses are due to the external electromagnetic field disregarding the distortion introduced by the induced currents in the conductive medium. Note that the low frequency range is equivalent to small values of the ratio r_0/δ because the penetration depth of the strand δ has large values.

The conduction losses can be obtained considering a uniform longitudinal electric field $E_z^0\hat{\mathbf{z}}$ equal to $(-V/l)\hat{\mathbf{z}}$. In this case, the current density carried by the strand is $\sigma E_z^0\hat{\mathbf{z}}$ uniformly distributed in the cross-section area, consequently the total current I_0 equals $\pi r_0^2\sigma E_0$. Finally, the conduction resistance per unit length is obtained dividing the electromotive force into the total current, obtaining the well known dc conduction resistance per unit length $R_{cond\,u.l.}^{low}$ expressed as follows:

$$R_{cond\,u.l.}^{low} = \frac{1}{\pi r_0^2\sigma}. \tag{24}$$

The previous result is equivalent to including the low frequency conduction factor $\Phi_{cond}^{low}(r_0/\delta)$ equal to one in (16).

The non-distorted electric field associated with an external transversal magnetic field $\mathbf{H}_t^0(\mathbf{r}_i)$ can be derived from (22) as:

$$\mathbf{E}_{\mathbf{H}_t^0}(\mathbf{r}) = j\omega\mu_0\rho\sin(\varphi - \varphi_0)H_t^0\hat{\mathbf{z}}. \tag{25}$$

Therefore, the proximity losses arising from the preceding electric field can be calculated by integrating the power loss, thus:

$$P_{prox,\,u.l.}^{low} = \pi\omega^2\mu_0^2\sigma r_0^4\bar{H}_t^2. \tag{26}$$

Rearranging the expression and applying the equivalence to the equivalent resistance, we obtain:

$$R_{prox\,t,\,u.l.}^{low} = \frac{4\pi}{\sigma}\Phi_{prox}^{low}(r_0/\delta)\bar{H}_t^2, \tag{27}$$

where we have:

$$\Phi_{prox}^{low}(r_0/\delta) = \frac{1}{4}\left(\frac{r_0}{\delta}\right)^4, \tag{28}$$

The values of $\Phi_{cond}^{low}(r_0/\delta)$ and $\Phi_{prox}^{low}(r_0/\delta)$ can also be obtained applying the small argument values to the complete functions shown

in (16) and (18), respectively, assuming the identity $J_n(z) \cong \frac{1}{n!}(\frac{z}{2})^n$ [47].

On the other hand, the high frequency limit power losses concern surface currents because electromagnetic fields exponentially decay inside the conductor for low values of δ with respect to the radius r_0, as is shown in [44, 45] for a flat half-space surface. Therefore, for a strand immersed in a uniform electric field $E_z^0(\mathbf{r}_i)\hat{\mathbf{z}}$, we have:

$$\mathbf{E}(\mathbf{r}) = E_z^0(\mathbf{r}_i)e^{-\frac{1+j}{\delta}\Delta}\hat{\mathbf{z}}, \tag{29}$$

where Δ is the distance to the strand surface equal to $R_0 - \rho$. The current density $\mathbf{J}_c$ can be approached by a surface current density $\mathbf{K}_c$ provided by the following expression:

$$\mathbf{K}_c \cong \int_0^\infty \sigma E_z^0(\mathbf{r}_i)e^{-\frac{1+j}{\delta}\Delta}d\Delta\hat{\mathbf{z}}, \tag{30}$$

hence:

$$\mathbf{K}_c \cong \frac{\sigma\delta}{1+j}E_z^0(\mathbf{r}_i)\hat{\mathbf{z}}. \tag{31}$$

As a result, the current I_0 carried by the strand is equal to:

$$I_0 \cong 2\pi r_0 \frac{\sigma\delta}{1+j}E_z^0(\mathbf{r}_i). \tag{32}$$

Considering that $E_z^0(\mathbf{r}_i)$ is $-V/l$, and applying the identity $R = \Re e(V/I)$, we have:

$$R_{cond,\,u.l.}^{high} \cong \frac{1}{2\pi r_0 \sigma \delta}. \tag{33}$$

In conclusion, we obtain the expression:

$$\Phi_{cond,\,u.l.}^{high}(r_0/\delta) = \frac{1}{2}\frac{r_0}{\delta}. \tag{34}$$

The factor $\Phi_{prox,\,u.l.}^{high}$ can be easily obtained starting with the configuration of the strand immersed in a uniform longitudinal magnetic field $H_z^0(\mathbf{r}_i)$ because the field is not distorted by the induced currents in the conductor. Additionally, considering the azimuthal electric field inside the strand with a dependence shown in (22) associated with a surface current similar to (31), together with the fact that the magnetic field vanishes inside the conductor, it is possible to define the so called impedance boundary condition [48–50] establishing the relationship between the tangential magnetic and electric field in the surface of the strand. In this case, it should be noted that both the

longitudinal electric field and the azimuthal electric field are tangential to the surface, thus:

$$Z_0 = \frac{E_\varphi(r_0)}{H_z^0(\mathbf{r}_i)} = \frac{1+j}{\sigma\delta}. \tag{35}$$

The electric field inside the strand also decays exponentially, as shown in (19). Consequently, the high frequency approach of the proximity power losses per surface unit $P_{prox\,z,\,u.s.}^{high}$ can be calculated by integrating the dissipated power density $\frac{1}{2}\mathbf{E}\cdot\mathbf{J}^*$ where the azimuthal electric field at the surface of the strand $E_\varphi(r_0)$ is $\frac{1+j}{\sigma\delta}H_z^0(\mathbf{r}_i)$. Thus, we have:

$$P_{prox\,z,\,u.s.}^{high} = \frac{1}{2}\int_0^\infty \frac{\left|H_z^0(\mathbf{r}_i)\right|^2}{\sigma\delta^2}e^{-\frac{2\Delta}{\delta}}\,d\Delta. \tag{36}$$

Integrating the above expression and multiplying by $2\pi r_0$ to calculate the power losses per unit length, we have:

$$P_{prox\,z,\,u.l.}^{high} = \frac{2\pi}{\sigma}\frac{r_0}{\delta}\left|H_z^0(\mathbf{r}_i)\right|^2. \tag{37}$$

As a result, the proximity factor at high frequencies is given by:

$$\Phi_{prox}^{high}(r_0/\delta) = \frac{r_0}{\delta}. \tag{38}$$

It should be noted that the expression for $\Phi_{cond}^{high}(r_0/\delta)$ and $\Phi_{prox}^{high}(r_0/\delta)$ can be derived from (16) and (18), respectively, considering the approximation for large argument values of the Bessel functions $J_n(z) \cong \sqrt{2/(\pi z)}\cos(z - \frac{1}{2}nz - \frac{1}{4}\pi)$ [47].

Figures 3(a) and 3(b) show the low- and high-frequency approaches compared with the complete expressions, respectively. The low frequency approach is accurate for the ratio up to one unit, whereas the high frequency approach can be used for ratios above several units.

5. EXPERIMENTAL VERIFICATION

The usefulness of the preceding expressions will be proven by being applied in a practical example consisting of the resistance calculation of a coil made with multi-stranded litz-wire. Two configurations are considered: first, an isolated coil placed in air and, second, a coil located above a magnetic flux concentrator which modifies the electromagnetic field, resulting in different resistance values. The total resistance is calculated by the addition of the different sources of power losses. Note that the ferrite layer acts as a current mirror increasing
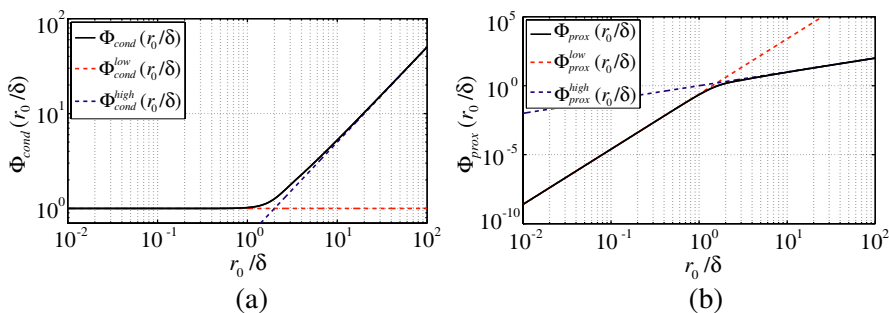
Figure 3. Comparison between complete expressions of conduction and proximity factors with respect to the low and high frequency approaches. (a) $\Phi_{cond}(r_0/\delta)$. (b) $\Phi_{prox}(r_0/\delta)$.
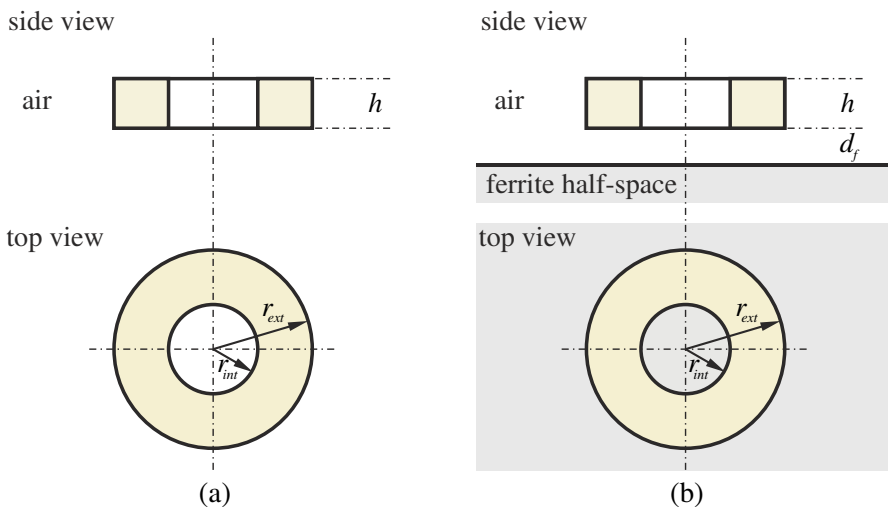

Figure 4. Geometrical structure of the two coil configurations experimentally measured. (a) Coil in air. (b) Coil above magnetic medium.

the magnetic field where the coil is immersed. As a consequence, the proximity losses increase.

The measurements have been performed for a ring-type coil of n turns of wire composed of n_0 strands with a radius r_0 evenly distributed in the cross-section area of the coil.

The geometrical characteristics of the circular coil are defined by the internal radius r_{int}, the external radius r_{ext}, and the height h, as

shown in Figure 4(a). The coil is modeled as a uniform current density distribution due to the strand radius r_0 and the distance between the strands being smaller than the coil dimension. As a consequence, an ideal coil placed in air can be electrically characterized by its own frequency-independent inductance L. The total resistance of this type of device is taken into account by the addition of the equivalent resistances associated with the conduction R_{cond} and proximity power losses R_{prox} in the winding.

Moreover, the second configuration is built adding a magnetic half-space placed below the coil at a distance d_f, as depicted in Figure 4(b).

The conduction losses are associated with a conduction resistance value R_{cond} calculated considering that the strands in the bundle are connected in parallel. Consequently, the expression for R_{cond} is the wire length $n\pi(r_{ext} - r_{int})$ multiplied by the conduction resistance $R_{cond\,u.l.}$ per unit length of the strands and divided by the number of strands n_0, as is expressed as follows [19]:

$$R_{cond} = \frac{1}{r_0^2 \sigma} \frac{n}{n_0} \Phi_{cond}(r_0/\delta)(r_{ext} - r_{int}). \tag{39}$$

On the other hand, the proximity resistance R_{prox} is calculated by the addition of the losses arising from the external magnetic field acting over each strand. Note that the proximity losses are only originated by the transversal magnetic field because the longitudinal magnetic field is null due to the geometrical symmetry of the system. Consequently, the expression for the proximity resistivity is given by [19]:

$$R_{prox} = \frac{8\pi^2}{\sigma} n n_0 \Phi_{prox}(r_0/\delta) \left\langle r \cdot \bar{H}_0^2 \right\rangle, \tag{40}$$

where ρ is the radial coordinate with respect to the coil axis and $\langle \rho \cdot \bar{H}_0^2 \rangle$ is the coil cross-section mean value of the product between ρ and $\bar{H}_0^2$. Note that the proximity losses depend on the square of the transversal magnetic field along the strands.

The configuration measured in Figure 4(a) is a toroidal coil with internal radius r_{int} of 21.5 mm, external radius r_{ext} of 29 mm and height h of 4 mm. The coil is made winding 24 turns of litz-wire composed of 35 strands of radius r_0 equal to 75 μm of copper with electric conductivity σ at room temperature of $5.8 \cdot 10^7$ S/m. On the other hand, in Figure 4(b), the configuration consists of the preceding coil placed above a magnetic half-space at a distance d_f of 1 mm which is made of a high-magnetic ferrite with relative magnetic permeability μ_r of 2000.

The measurements have been performed by means of a precision LCR-meter Agilent E4940A at frequencies ranging from 1 kHz to
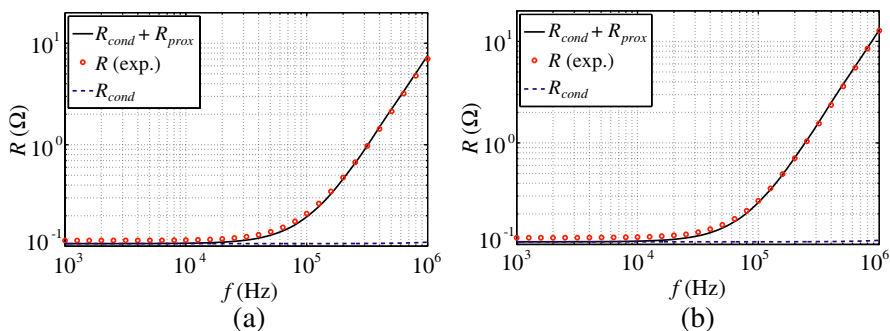
Figure 5. Experimental measurements and numerical results for a 24 turn coil in air and placed above a ferrite layer. Conduction resistances are also represented and the additional resistance is associated with proximity losses. (a) Coil in air. (b) Coil above ferrite layer.

1 MHz. Note that each frequency is associated with a penetration depth δ value of the strand. The output data is the equivalent impedance provided in equivalent resistance and inductance terms. Basically, the inductance depends on the system geometry having a weak relation with the internal structure of the wire. The inductance is almost constant in the overall frequency range in both cases, but is higher for the second configuration due to the presence of the magnetic layer. On the other hand, the resistance is due to the power losses in the winding because the dissipation in the remaining components of the system is negligible. Thus, the total resistance equals the sum of the conduction resistance R_{cond} and the proximity resistance R_{prox}.

Figures 5(a) and 5(b) show a good agreement between the experimental results and the numerical based values calculated with the addition of the conduction resistance obtained applying (39) and the proximity resistance from (40). In both cases, at the low frequency range, the conduction losses dominate. As a result, the value of the total resistance is essentially constant and no influence of the flux concentrator is observed because the conduction losses are independent of the magnetic field. On the other hand, at the high frequency range, the measured resistance is almost totally originated by the proximity losses. Thus, the total resistance greatly depends on the frequency and, additionally, the resistance is modified by the flux concentrator. Considering the previous analysis, the conduction resistance R_{cond} is almost constant in the whole frequency range, whereas the proximity resistance R_{prox} becomes the most important contribution above several tens of kHz.

6. CONCLUSION

The power losses in the winding of magnetic devices used in power systems made with multi-stranded litz-wire are analyzed in depth in this paper. A unified approach is developed for the different types of losses, either conduction or proximity losses. Moreover, external electromagnetic fields are considered as the sources modeling the effects of the complete system in the winding. The external electromagnetic field is decomposed into transversal magnetic TM and transversal electric TE components along the direction of the wire. The traditional power losses in the winding, called conduction and proximity losses, have been associated with a uniform longitudinal electric field and a transversal magnetic field, respectively. In this paper the relationship with the zeroth and first order TM modes have been established in order to achieve a unified analysis of the loss contributions. Additionally, the proximity losses due to the longitudinal magnetic field have been included by the action of the zeroth order TE mode. Both proximity loss contributions possess similar analytical expressions except for a proportional factor doubling the effect of the transversal magnetic field $\mathbf{H}_t^0(\mathbf{r}_i)$ with respect to the longitudinal magnetic field $H_z^0(\mathbf{r}_i)\hat{\mathbf{z}}$.

It is worth noting that the power losses in the winding are always related with the electric field of the analyzed mode because the losses are due to the electric currents in the strands. As a consequence, the external field originating the power losses in the winding can be substituted by an impressed current equivalent to the product between the conductivity of the strand and the electric field of the considered mode. As a result, the power losses can be easily evaluated. It should be noted that the evaluation at high frequencies includes the effect of the field distortion due to the conduction of the strand.

The analysis of power losses can be simplified taking into account the behavior of the system depending on the excitation frequency, which can be divided into a low- and high-frequency range depending on the value of the ratio r_0/δ. The low frequency ranges from dc to frequencies where r_0/δ is up to one unit, whereas at the high frequency limit r_0/δ is above several units. On the one hand, in the low frequency approach the external field is not distorted by the strand. On the other hand, in the high frequency approach the current densities in the strand become surface currents and the surface electric field and magnetic fields can be related by means of the so called impedance boundary conditions. It should be noted that simple expressions of power losses can be easily derived with an extended range of validity. Moreover, these approaches allow further analysis of more complex

cross-section strand geometries where it is impractical to obtain exact analytical expressions.

Finally, the expressions obtained have been experimentally verified for two simple coil systems. The cases considered exhibit a high symmetric configuration, and therefore the power losses are only due to the TM modes. However, the power losses in less symmetric systems, for instance transformers or inductors used in commercial domestic heaters, should be accounted for by considering the additional TE contribution originated by the longitudinal magnetic field $H_z^0(\mathbf{r}_i)\hat{\mathbf{z}}$.

ACKNOWLEDGMENT

REFERENCES

1. Lammeraner, J. and M. Stafl, *Eddy Currents*, Chemical Rubber Co., Cleveland, Ohio, 1964.

2. Urling, A. M., et al., "Characterizing high-frequency effects in transformer windings — A guide to several significant articles," *Applied Power Electronics Conference*, 373–385, Baltimore, USA, 1989.

3. Reatti, A. and M. K. Kazimierczuk, "Comparison of various methods for calculating the AC resistance of inductors," *IEEE Transactions on Magnetics*, Vol. 38, No. 3, 1512–1518, 2002.

4. Nan, X. and C. R. Sullivan, "An improved calculation of proximity-effect loss in high-frequency windings of round conductors," *Power Electronics Specialist Conference*, 853–860, Acapulco, Mexico, 2003.

5. Dowell, P. L., "Effects of eddy currents in transformer windings," *Proceedings of the Institution of Electrical Engineers*, Vol. 113, No. 8, 1387–1394, 1966.

6. Robert, F., "A theoretical discussion about the layer copper factor used in winding losses calculation," *IEEE Transactions on Magnetics*, Vol. 38, No. 5, 3177–3179, 2002.

7. Sippola, M. and R. E. Sepponen, "Accurate prediction of high-frequency power-transformer losses and temperature rise," *IEEE Transactions on Power Electronics*, Vol. 17, No. 5, 835–847, 2002.

8. Acero, J., et al., "A model of losses in twisted-multistranded wires for planar windings used in domestic induction heating

appliances," *Applied Power Electronics Conference*, 1247–1253, Anaheim, USA, 2007.

9. Lotfi, A. W. and F. C. Lee, "A high frequency model for Litz wire for switch-mode magnetics," *Industry Applications Society Annual Meeting*, 1169–1175, Toronto, Canada, 1993.

10. Ferreira, J. A., "Analytical computation of AC resistance of round and rectangular litz wire windings," *IEE Proceedings B, Electric Power Applications*, Vol. 139, No. 1, 21–25, 1992.

11. Lotfi, A. W., P. M. Gradzki, and F. C. Lee, "Proximity effects in coils for high frequency power applications," *IEEE Transactions on Magnetics*, Vol. 28, No. 5, 2169–2171, 1992.

12. Albach, M., "Two-dimensional calculation of winding losses in transformers," *Power Electronics Specialists Conference*, 1639–1644, Galway, Ireland, 2000.

13. Tourkhani, F. and P. Viarouge, "Accurate analytical model of winding losses in round Litz wire windings," *IEEE Transactions on Magnetics*, Vol. 37, No. 1, 538–543, 2001.

14. Spang, M. and M. Albach, "Optimized winding layout for minimized proximity losses in coils with rod cores," *IEEE Transactions on Magnetics*, Vol. 44, No. 7, 1815–1821, 2008.

15. Larouci, C., et al., "Copper losses of flyback transformer: Search for analytical expressions," *IEEE Transactions on Magnetics*, Vol. 39, No. 3, 1745–1748, 2003.

16. Kazimierczuk, M. K., *High-frequency Magnetic Components*, John Wiley & Sons Ltd, Chichester, UK, 2009.

17. Perry, M. P., "On calculating losses in current carrying conductors in an external alternating magnetic field," *IEEE Transactions on Magnetics*, Vol. 17, No. 5, 2486–2488, 1981.

18. Fawzi, T. H., P. E. Burke, and B. R. McLean, "Eddy losses and power shielding of cylindrical shells in transverse and axial magnetic fields," *IEEE Transactions on Magnetics*, Vol. 31, No. 3, 1452–1455, 1995.

19. Carretero, C., R. Alonso, J. Acero, O. Lucia, and J. M. Burdio, "Dissipative losses evaluation in magnetic power devices with litz-wire type windings," *PIERS Online*, Vol. 7, No. 3, 246–250, 2011.

20. Namjoshi, K. V., J. D. Lavers, and P. P. Biringer, "Eddy current power loss in structural steel due to cables carrying current in a perpendicular direction," *IEEE Transactions on Magnetics*, Vol. 30, No. 1, 85–91, 1994.

21. Sullivan, C. R., "Optimal choice for number of strands in a litz-wire transformer winding," *IEEE Transactions on Power*

Electronics, Vol. 14, No. 2, 283–291, 1999.

22. Sullivan, C. R., "Computationally efficient winding loss calculation with multiple windings, arbitrary waveforms, and two-dimensional or three-dimensional field geometry," *IEEE Transactions on Power Electronics*, Vol. 16, No. 1, 142–150, 2001.

23. Nan, X. and C. R. Sullivan, "Simplified high-accuracy calculation of eddy-current loss in round-wire windings," *Power Electronics Specialists Conference*, 873–879, Aachen, Germany, 2004.

24. Koertzen, H. W. E., J. D. van Wyk, and J. A. Ferreira, "An investigation of the analytical computation of inductance and AC resistance of the heat-coil for induction cookers," *Industry Applications Society Conference*, 1113–1119, Houston, USA, 1992.

25. Acero, J., et al., "Frequency-dependent resistance in litz wire planar windings for domestic induction heating appliances," *IEEE Transactions on Power Electronics*, Vol. 21, No. 4, 856–866, 2006.

26. Hernandez, P., et al., "Power losses distribution in the litz-wire winding of an inductor for an induction cooking appliance," *Conference of the Industrial Electronics Society*, 1134–1137, Sevilla, Spain, 2002.

27. Podoltsev, A. D., I. N. Kucheryavaya, and B. B. Lebedev, "Analysis of effective resistance and eddy-current losses in multiturn winding of high-frequency magnetic components," *IEEE Transactions on Magnetics*, Vol. 39, No. 1, 539–548, 2003.

28. Dular, P. and J. Gyselinck, "Modeling of 3-D stranded inductors with the magnetic vector potential formulation and spatially dependent turn voltages of reduced support," *IEEE Transactions on Magnetics*, Vol. 40, No. 2, 1298–1301, 2004.

29. Gyselinck, J. and P. Dular, "Frequency-domain homogenization of bundles of wires in 2-D magnetodynamic FE calculations," *IEEE Transactions on Magnetics*, Vol. 41, No. 5, 1416–1419, 2005.

30. Gyselinck, J., R. V. Sabariego, and P. Dular, "Time-domain homogenization of windings in 2-D finite element models," *IEEE Transactions on Magnetics*, Vol. 43, No. 4, 1297–1300, 2007.

31. Sabariego, R. V., P. Dular, and J. Gyselinck, "Time-domain homogenization of windings in 3-D finite element models," *IEEE Transactions on Magnetics*, Vol. 44, No. 6, 1302–1305, 2008.

32. Kong, J. A., "Electromagnetic fields due to dipole antennas over stratified anisotropic media," *Geophysics*, Vol. 37, No. 6, 985–996, 1972.

33. Clemmow, P. C., "The resolution of a dipole field into transverse electric and transverse magnetic waves," *Proceedings of the*

Institution of Electrical Engineers, Vol. 110, No. 1, 107–111, 1963.

34. Wilton, D., "A TM-TE decomposition of the electromagnetic field due to arbitrary sources radiating in unbounded regions," *IEEE Transactions on Antennas and Propagation*, Vol. 28, No. 1, 111–114, 1980.

35. Lindell, I. V., "TE/TM decomposition of electromagnetic sources," *IEEE Transactions on Antennas and Propagation*, Vol. 36, No. 10, 1382–1388, 1988.

36. Weiss, S. J. and W. K. Kahn, "Decomposition of electromagnetic boundary conditions at planar interfaces with applications to TE and TM field solutions," *IEEE Transactions on Antennas and Propagation*, Vol. 46, No. 11, 1687–1691, 1998.

37. Janaswamy, R., "A note on the TE/TM decomposition of electromagnetic fields in three dimensional homogeneous space," *IEEE Transactions on Antennas and Propagation*, Vol. 52, No. 9, 2474–2477, 2004.

38. Fawzi, T. H. and P. E. Burke, "Use of surface integral equations for analysis of TM-induction problem," *Proceedings of the Institution of Electrical Engineers*, Vol. 121, No. 10, 1109–1116, 1974.

39. Fawzi, T. H., P. E. Burke, and M. Fabiano-Alves, "Use of surface-integral equations for the analysis of the TE-induction problem," *Proceedings of the Institution of Electrical Engineers*, Vol. 123, No. 7, 725–728, 1976.

40. Carretero, C., R. Alonso, J. Acero, and J. M. Burdio, "Coupling impedance between planar coils inside a layered media," *Progress In Electromagnetics Research*, Vol. 112, 381–396, 2011.

41. Carcione, J. M., "Simulation of electromagnetic diffusion in anisotropic media," *Progress In Electromagnetics Research B*, Vol. 26, 425–450, 2010.

42. Rothwell, E. J. and M. J. Cloud, *Electromagnetics*, CRC Press, Boca Raton, 2000.

43. Ferreira, J. A., "Improved analytical modeling of conductive losses in magnetic components," *IEEE Transactions on Power Electronics*, Vol. 9, No. 1, 127–131, 1994.

44. Silveira, F. E. M. and J. A. S. Lima, "Skin effect from extended irreversible thermodynamics perspective," *Journal of Electromagnetic Waves and Applications*, Vol. 24, Nos. 2–3, 151–160, 2010.

45. Voyer, D., R. Perrusel, and P. Dular, "Perturbation method for the calculation of losses inside conductors in microwave structures," *Progress In Electromagnetics Research*, Vol. 103, 339–

354, 2010.

46. Burke, P., T. Fawzi, and T. Akinbiyi, "The use of asymptotes to estimate TE- and TM-mode losses in long conductors," *IEEE Transactions on Magnetics*, Vol. 14, No. 5, 374–376, 1978.

47. Abramowitz, M. and I. A. Stegun, *Handbook of Mathematical Functions: With Formulas, Graphs, and Mathematical Tables*, U.S. Dept. of Commerce, Washington, D.C., 1970.

48. Qian, Z.-G., M.-S. Tong, and W. C. Chew, "Conductive medium modeling with an augmented GIBC formulation," *Progress In Electromagnetics Research*, Vol. 99, 261–272, 2009.

49. Fawzi, T., M. Ahmed, and P. Burke, "On the use of the impedance boundary conditions in eddy current problems," *IEEE Transactions on Magnetics*, Vol. 21, No. 5, 1835–1840, 1985.

50. Yuferev, S. and N. Ida, *Surface Impedance Boundary Conditions. A Comprehensive Approach*, CRC Press, Boca Raton, 2009.